mater.scichina.com link.springer.com

Published online 1 January 2023 | https://doi.org/10.1007/s40843-022-2286-5
Sci China Mater 2023, 66(4): 1539–1550

An ultra-tough and super-stretchable ionogel with multi functions towards flexible iontronics

Weiqing Zhan[1], Haoqi Zhang[1], Xiaolin Lyu[1*], Zhong-Zhen Luo[1*], Yan Yu[1] and Zhigang Zou[1,2]

ABSTRACT Ionogels have attracted much attention in recent years because of their good thermal stability, high ionic conductivity, and non-volatility. However, there is a trade-off between the mechanical strength and stretchability of ionogels, which results in unsatisfactory mechanical performance. Herein, strong polymer crystallization and weak ion-dipole interaction are combined to prepare an ultra-tough and super-stretchable ionogel. The crystalline region can dissipate the energy through the stress-induced disaggregation mechanism in the stretching process and toughen the gel, while the reversible formation and dissociation of the ion-dipole interaction between amorphous polymer chains and ionic liquids can provide elasticity for large strain. These ionogels have high toughness, strong tensile strength, large Young's modulus, and good stretchability. Furthermore, the ionogels also possess other properties like good fatigue resistance, quick self-recovery, high transparency, recyclability, self-healing ability, high ionic conductivity, and wide electrochemical window. This ionogel exhibits great potential in several iontronic devices, such as triboelectric nanogenerators, ionic thermoelectric materials, and strain sensors. This study develops a new method to guide the preparation of high-performance ionogels by combining reversible strong and weak interactions.

Keywords: tough ionogel, flexible iontronics, ionic thermoelectric, strain sensor

INTRODUCTION

Flexible conductive materials have attracted much attention in recent years because of their potential applications in ionic skins, energy conversion, flexible displays, etc. [1–5]. Soft ionic conductors, such as hydrogels, show great advantages in flexible devices due to their excellent mechanical properties, high ionic conductivity, and good transparency [6–8]. In the last decade, a great many strategies have been proposed to prepare hydrogels with outstanding strength and stretchability. The basic principle is to design the molecular structure for achieving the dissipation of energy and high deformation of gels. The reason for the extraordinary mechanical properties of well-known double network hydrogels is that the rigid and brittle network can dissipate the energy, while the flexible and elastic network can provide great deformation [9–11]. However, the dehydration of hydrogels at elevated temperatures and crystallization of water below 0°C restrict many applications. Although some organic solvents and hygroscopic salts were used to alleviate these problems, such actions are palliatives [12].

Ionic liquids (ILs) are room-temperature molten salts composed of mobile cations and anions [13]. They have received increasing interest in many fields because of their high ionic conductivity, electrochemical stability, nonvolatility, and non-flammability [14–16]. IL-based gels, or called ionogels, can retain many advantages of ILs and polymers. Up to now, although many strategies have been developed to prepare super-stretchable ionogels (elongation at break >1000%), most ionogels still have unsatisfactory mechanical performances, like low tensile strength (<1 MPa), low toughness (<0.1 kJ m^{-2}) and low Young's modulus (<0.1 MPa), which are far lower than those of their hydrogel counterparts with the tensile strength, toughness and modulus of ~7 MPa, ~40 kJ m^{-2} and ~210 MPa, respectively. Generally, The chemically or physically crosslinked network can strengthen the skeleton framework by incorporating crosslinking points [17–19]. Chemical crosslinking can greatly enhance the rigidity of the network, which can increase the stress at break. However, the increased rigidity will damage the elasticity of polymer chains, and the ionogel cannot be stretched to the extent of satisfaction [20]. Due to the poor mechanical properties of ionogels based on poly(vinylidene fluoride-*co*-hexafluoropropylene) (PVDF-*co*-HFP) with a high VDF content, Shi's group [21] introduced a chemical cross-linking network in PVDF-*co*-HFP gels by a double-network approach to inhibit the strain-induced crystallization of PVDF-*co*-HFP, which could improve the fracture stress (2.2 MPa), but its elongation at break is still small (307%). For physically crosslinked ionogels, most physical crosslinking points are too weak to ensure enough mechanical strength [22,23]. For example, Wang's group [24] obtained an ionogel with excellent stretchability and self-healing properties by regulating the ion-dipole interaction in PVDF-*co*-HFP fluoroelastomer with a low VDF content, but its fracture stress was low (0.11 MPa). To prepare tough and stretchable ionogels, different interactions (such as electrostatic interaction, ion-dipole interaction, and hydrogen bonding) were also grouped to dissipate the energy in the stretching process and increase the elasticity of polymer chains [24–30]. However, it is still a challenge to prepare ionogels with excellent mechanical properties.

Herein, we propose that the polymer crystallization and ion-

[1] Key Laboratory of Advanced Materials Technologies, International (Hong Kong, Macao and Taiwan) Joint Laboratory on Advanced Materials Technologies, College of Materials Science and Engineering, Fuzhou University, Fuzhou 350108, China
[2] Eco-materials and Renewable Energy Research Center, College of Engineering and Applied Sciences, Nanjing University, Nanjing 210093, China
[*] Corresponding authors (emails: lyuxiaolin@fzu.edu.cn (Lyu X); zzluo@fzu.edu.cn (Luo ZZ))

dipole interactions in PVDF-*co*-HFP can be controlled to regulate the mechanical properties of ionogels. The content of VDF in the selected PVDF-*co*-HFP was 88 mol%. Then, the fracture stress and elongation at the break of the ionogel can be simultaneously improved when the crystallization and ion-dipole interactions reach equilibrium, which will not fracture easily or have low strength. The strong crystalline interactions can dissipate energy like brittle networks during stretching, while the weak ion-dipole interaction can provide elasticity for ionogels like elastic networks, which can solve the trade-off between the strength and stretchability of the ionogels. Meanwhile, it is found that the reversible disaggregation and recrystallization behaviors in the stretching and recovery processes play an important role in promoting the mechanical properties by *in situ* small-angle X-ray scattering (SAXS) and wide-angle X-ray scattering (WAXS). The gels have high fracture toughness, strong tensile strength, large Young's modulus, as well as good tensile elongation at break. On the other hand, many properties, such as high ionic conductivity, good fatigue resistance, quick self-recovery, high transparency, recyclability, and self-healing capability, are also possessed to expand the applicability of the ionogel. To illustrate the applications in wearable devices, we studied its potential in the fields such as triboelectric nanogenerators, ionic thermoelectric materials, and strain sensors.

EXPERIMENTAL SECTION

Materials

1-Ethyl-3-methylimidazolium bis(trifluoromethyl sulfonyl) imide (EMIm TFSI) was purchased from Sigma-Aldrich. PVDF-*co*-HFP with 88 mol% VDF was obtained from Arkema Group (Kynar Flex 2801). Fluoroelastomer with 78 mol% VDF and PVDF-*co*-HFP with 96 mol% VDF as the control group were purchased from 3M Co. (Dyneon FE 5640Q) and Sigma-Aldrich, respectively. Dimethyl formamide (DMF) was provided by Shanghai Aladdin Biochemical Technology Co., Ltd. All reagents were used without purification unless otherwise indicated.

Preparation of ionogels

PVDF-*co*-HFP was dissolved in DMF by stirring for 3 h to obtain a homogeneous clarified solution with the polymer mass fraction of ~10 wt%. The calculated amount of IL was added into the solution followed by stirring for another 2 h. The mixed solution was then poured into a polytetrafluoroethylene (PTFE) mold. After the organic solvent was evaporated in the fume hood, the mold was further placed in a vacuum oven at 80°C to remove all solvent. The ionogels as the control group were prepared similarly. The obtained ionogel sample was further cut into different shapes for the corresponding experiments.

Mechanical properties

The mechanical properties of ionogels were measured using a universal testing machine (Xiamen Meitesi Instrument). The ionogel film was cut into a dumbbell shape, with a length of 40 mm, a width of 8 mm, and a thickness of 0.5 mm, to perform the tensile and cyclic stress-strain experiments. The stretching rate of the tensile test was fixed at 10 mm min^{-1} unless otherwise indicated. The mechanical tests of each weight fraction were repeated in three batches and each batch had four samples. In the self-healing test, the dumbbell-shaped sample was cut into half and healed at 120°C. Then, the healed sample was used to conduct the tensile stress-strain experiment. The ionogel with a trouser shape (length 40 mm, width 10 mm, thickness 0.5 mm) and an initial cut of 20 mm was used to carry out the tearing test [31]. Fracture energy, or toughness, was calculated using the equation $T = 2F_{av}/w$, where F_{av} is the median value of peak forces and w is the thickness of the sample. Rheological measurements were performed on a rheometer (Anton Paar MCR302, Austria). Dynamic frequency sweep measurement was performed in the range from 10^{-1} to 10^{2} rad s^{-1} at a fixed shear strain of 1% at 25°C. Temperature sweep measurement was performed in the temperature range from 25 to 140°C at a fixed angular frequency of 10 rad s^{-1}, a fixed shear strain of 1%, and a heating rate of 2°C min^{-1}.

Structural analysis

The transmittance of ionogels in the visible light range was measured by an ultraviolet (UV)-visible spectrophotometer (UV-LAMBDA 950, PerkinElmer) with a sample thickness of 0.5 mm. The Fourier transform infrared (FTIR) results were obtained using Nicolet iS 10. Scanning electron microscopy (SEM) results were acquired on a Supra 55 sapphire SEM at an acceleration voltage of 10 kV. WAXS and SAXS experiments were carried out on the Ganesha SAXS Lab. The *d*-spacing values of scattering peaks were calculated through the equation $d = 2\pi/q$ [32–35]. The Peakfit software (Systat Software Inc.) was used to split the crystalline peak from the amorphous halo in the WAXS profile. The averaged domain size of the crystallites was then approximately determined by the Scherrer's equation: $D = (K \times \lambda)/(\beta_{2\theta} \times \cos\theta_0)$, where D is the averaged domain size of the crystallites perpendicular to a particular *hkl* plane, K (~0.89) and λ (0.154 nm) are the Scherrer shape factor and X-ray wavelength, respectively, $\beta_{2\theta}$ is full width at half maximum intensity of the peak corresponding to the *hkl* plane, and θ_0 is the center of the diffraction peak. The *d*-spacing value was calculated by the Bragg's equation ($2d\sin\theta_0 = \lambda$).

Thermal properties

Thermal gravimetric analysis (TGA) was carried out to investigate the thermal stability of ionogels on an STA449C instrument with a heating rate of 10°C min^{-1} from ambient temperature to 600°C under nitrogen. Differential scanning calorimetry (DSC) measurements were conducted using a DSC 214 Polyma to analyze the thermal properties of ionogels with the heating rate of 10°C min^{-1} from 0 to 170°C under nitrogen. The degree of PVDF crystallinity in ionogels was estimated using the equation below:

$$X_c(\%) = \frac{\Delta H_f}{\Delta H_m^0} \times 100\%,$$

where ΔH_f represents the fusion enthalpy of the crystalline domain in the ionogel calculated by the melting peak in the DSC profile, and ΔH_m^0 represents the standard fusion enthalpy of 100% PVDF crystal. According to the literature [36], the ΔH_m^0 value of 104.7 J g^{-1} is adopted.

Electrical properties

The electrical properties of the ionogel were characterized by an electrochemical station (CHI660e, CH Instrument). The ionogel with a thickness of 0.5 mm was cut into a circle shape and sandwiched between two stainless steel electrodes with a dia-

meter of 2 cm. The electrochemical impedance spectrum (EIS) was measured with a frequency range from 1 Hz to 1 MHz and an amplitude of 5 mV. The obtained Nyquist plot was then used to determine the bulk resistance (R). And the ionic conductivity (σ) was calculated by the formula $\sigma = L/(R \times A)$, where L and A represent the distance between two electrodes and the cross-sectional area of the ionogel film, respectively. The electrochemical window of the ionogel was evaluated by linear sweep voltammetry with a potential range of 0–5 V and a scanning speed of 0.01 V s^{-1}.

Applications

The real-time resistance of the ionogel-based strain sensor was recorded using a Keithley 2601b source meter. The relative resistance change was calculated using the equation $\Delta R/R_0 = R/R_0 - 1$, where R and R_0 were the resistances of the ionogel in the pristine and stretched states, respectively. Then, the performance of the sensor was also assessed by placing the ionogel on different joints of the body to monitor the body movements. The ionic triboelectric nanogenerator (iTENG) was fabricated by placing a 3M VHB tape (electrification layer) on the ionogel film (electrode layer). The electrical signals were generated by touching the electrification layer using hands and recorded by the Keithley 2601b source meter. The thermopower was determined by measuring the open-circuit voltages at different temperature gradients. And the thermopower was calculated using the equation $S_i = \Delta V/\Delta T$, in which ΔV and ΔT represent the open-circuit voltage and temperature difference, respectively. Two Peltier chips produced the temperature difference with the cold end fixed at 25°C. The open-circuit voltage was measured using the electrochemical station, and the temperature difference was measured by the thermocouples.

RESULTS AND DISCUSSION

Preparation of the ionogel

The key in the design of this ionogel is to balance different interactions for crosslinking polymer chains. Polymer crystallization is often used to create polymer gels with high strength, but this type of ionogel shows poor stretchability, which results from the destruction of large crystal domains [37]. Ion-dipole interaction between IL and fluorinated polar groups can endow ionogels with high stretchability and self-healing capability, but the mechanical strength of the ionogel is weak [24,38]. Therefore, an ionogel with high strength and stretchability can be obtained by balancing the polymer crystallization and ion-dipole interaction. These two interactions play an important role as strong bonds and weak bonds for the mechanical properties of the ionogel. The strong bonds can keep the shape of the ionogel and increase the mechanical strength, while the weak bonds can provide high stretchability and enhance the fatigue resistance by bond re-formation. Therefore, the ionogel with multiple interactions can become tough and stretchable in a similar way to polyampholyte hydrogels, although the inside topological structures are different [39,40]. The selection of the polymer matrix is PVDF-*co*-HFP. It is known that the ordered packing of PVDF can be destroyed by copolymerizing the HFP comonomer [41]. Therefore, increasing HFP content can reduce the degree of PVDF crystallinity and influence the type of the crystalline phase, which then affects the properties of the copolymer, such as melting temperature, mechanical strength, and the interaction with IL. Meanwhile, increasing HFP content can also reduce the domain size of PVDF crystallites, and the amorphous polar region can be plasticized by IL to form the ion-dipole interaction. When the VDF content is high, the ionogel is easy to fracture; while the fracture strength of the ionogel will be too low with a low VDF content [21,24]. Therefore, we choose a VDF content of 88 mol%. Then, the ionogel can be cross-linked by the uniformly dispersed crystallites and ion-dipole interaction.

To prepare the ionogel, EMIm TFSI, a widely used stable IL, was adopted. The ionogels can be prepared through solution casting (Fig. 1a). The squeezing test was carried out to ensure no leakage of IL, indicating the effective confinement of IL in the polymer matrix (Fig. S1). The content of IL varies from 30 to 80 wt% to adjust the mechanical and electrical properties of the ionogels. The ionogels with different IL contents all exhibit remarkable transparency (Figs S2 and S3). When the IL content is 80 wt%, the ionogel has the highest transparency of 93% (Fig. 1b). Meanwhile, this sample can be arbitrarily twisted and stretched to >500% using hands (Fig. 1c), and it can easily carry a weight of 0.5 kg (Fig. 1d). Compared with the ionogels prepared using PVDF-*co*-HFP with different VDF ratios, it can be found that the fluoroelastomer (78 mol% VDF content)-based ionogel with 80 wt% IL cannot form a freestanding film (Fig. S4), while the ionogels with VDF content of 96 mol% have poor tensile strength and low stretchability (Fig. S5). However, our ionogels show superior mechanical properties.

Characterization of mechanical properties

The TGA result reveals that the obtained ionogel has good thermal stability (Fig. 2a and Fig. S6). TG-mass spectrum (TG-MS) analysis reveals that there is no solvent inside (Fig. S7). DSC results show that these ionogels have low glass transition temperatures (T_g, Fig. S8). The higher the IL content, the lower T_g of the ionogel. The rheological results confirm that the ionogels exhibit solid-like elastic behavior, in which G' is greater than G'' over the entire angular frequency range from 10^{-1} to 10^2 rad s^{-1} (Fig. S9a, b). Then, the temperature sweep analysis was further conducted using the ionogel with 80 wt% IL (Fig. S9c). When the temperature is below 90°C, the storage and loss moduli of the ionogel remain unchanged. However, with further increasing temperature, the ionogel will undergo a gel-sol transition and the modulus will sharply decrease. The transition temperature is about 105°C.

With increasing polymer content, the tensile strength of the ionogel is increased from 2.2 to 11.7 MPa, accompanied by the significant increase of Young's modulus from 1.4 to 72.2 MPa, while the elongation at break is decreased from 1650% to 690% (Fig. 2b and Table S1). It is also remarkable that the ionogels still have high stretchability at higher stretching rates (Fig. 2c, Fig. S10, and Video S1). Meanwhile, when the environmental temperature is increased to 60°C, the elongation of the ionogel will be increased as well (Fig. S11). The tearing test exhibits that the fracture toughness has a positive relation with Young's modulus (Fig. 2d and Fig. S12). The toughness of the ionogel with 30 wt% IL is 37.5 kJ m^{-2}, which is higher than the previously reported best value (23.3 kJ m^{-2}) [31]. Moreover, the ionogel remains stable in the air because PVDF-*co*-HFP and EMIm TFSI are both hydrophobic (Fig. 2e). The cyclic tensile stress-strain test of the ionogel under different strains reveals the mechanical hysteresis and strain softening behavior (Fig. 2f). The higher the deformation, the bigger the dissipated energy

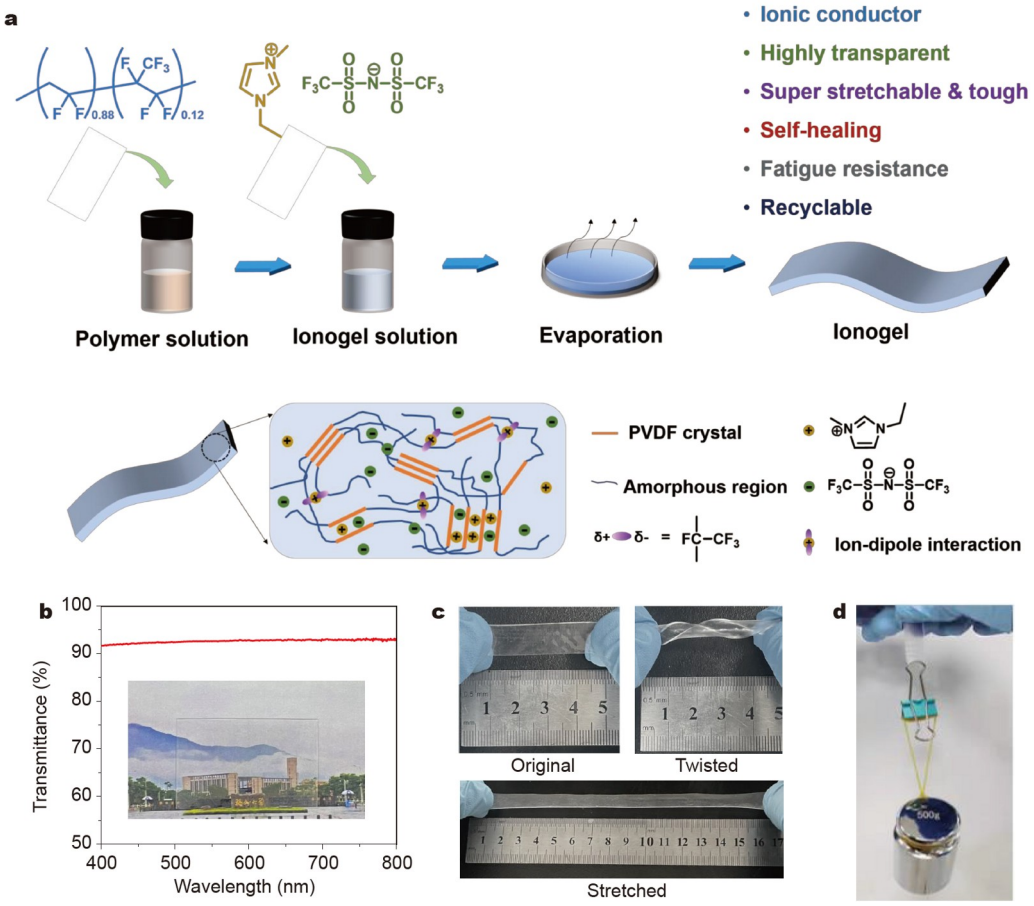

Figure 1 (a) Schematic of the preparation process and microstructure of the ionogel through the solution casting method. The ionogel is composed of crystalline and amorphous regions. (b) Transmittance spectrum of the ionogel (thickness: 0.5 mm) with the inset photograph showing the ionogel film over an image. (c) Photographs of the ionogel in the original, twisted, and stretched states. (d) Photograph of the ionogel lifting a weight of 0.5 kg.

(Fig. S13a). These features are typical characteristics of tough materials. The cyclic tensile behavior of the ionogel at a fixed strain shows that the dissipated energy is rapidly decreased after the first loading-unloading process, which means internal destruction appears (Fig. S13b). Further increasing the cycle counts will hardly influence the dissipated energy (Fig. S13c). The cyclic tensile behavior of the ionogel with 70 wt% IL is similar to that of the ionogel with 80 wt% IL, which means the ionogels have similar microstructures (Fig. S14). In the stretching process, the crystalline region can offer rigidity for the gel, and the destruction of crystallites can dissipate most energy of the stretching. Then, the elasticity of the amorphous region can provide high deformation of the network. The crystallization of PVDF, ion-dipole interaction, and polymer chain entanglement all contribute to the energy dissipation in the stretching process, which will be discussed in detail below. Young's modulus, toughness, elongation at break, and fracture stress of various gels, natural rubber, and cartilage are summarized in Fig. 2g–i [10,27,28,40,42–53]. Through the comparison and analysis, it can be found that our work greatly improves the mechanical strength of ionogels while keeping the super-stretchability. The overall performance of our ionogels exceeds most existing iono- and hydro-gels. Due to the similar mechanical strength to natural rubber and cartilage, the application of ionogels may be further extended from soft ionic conductors to structural materials.

Study of performance enhancing mechanism

To further reveal the enhancing mechanism of the ionogel from a microscopic point of view, a structural analysis was conducted. According to the WAXS experiments, it can be found that the diffraction peaks of the pure PVDF-*co*-HFP are different from those of PVDF-*co*-HFP with higher VDF contents in the literature (Fig. 3a) [54]. The diffraction peaks corresponding to the α-phase crystal of PVDF are completely suppressed, while a strong diffraction peak belonging to the β-phase crystal of PVDF, which is located at the 2θ value of 20.4°, is observed. With increasing IL content, the crystalline peaks of PVDF in ionogels will be further suppressed (Fig. 3a). When the IL content exceeds 60 wt%, a new peak at 12.6° appears in the WAXS profile, which may originate from the intercalation of IL ions in the crystallites [37,55]. Through peak fitting to separate the crystalline peak of the β-phase, the averaged domain size of the crystallites in the pure PVDF-*co*-HFP is calculated to be 5.2 nm using the Scherrer equation (Table S2). The averaged domain size is further decreased to 2.7 nm with increasing IL content to 80 wt%. Compared with that in the literature, the domain size of the crystallites is much smaller, which is also in accordance with the high transparency of the ionogels [21,36]. According to DSC results, the melting and crystallization

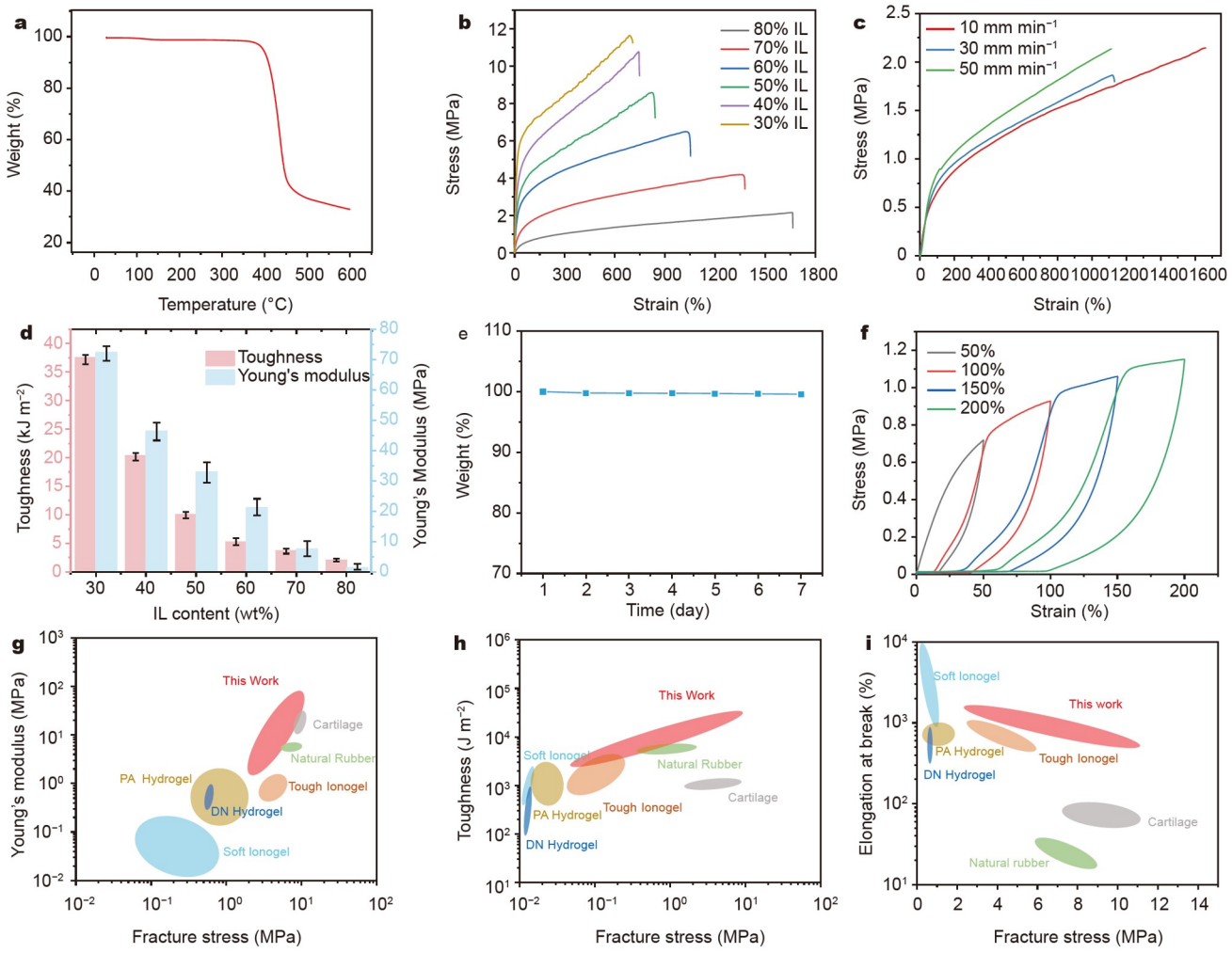

Figure 2 (a) TGA result of the ionogel with 80 wt% IL. (b) Tensile stress-strain curves of the ionogel with different IL contents at the stretching rates of 10 mm min^{-1}. (c) Tensile stress-strain curves of the ionogel with 80 wt% IL at different stretching rates. (d) Toughness and Young's modulus at different IL contents. (e) Weight-time dependence of the ionogel. (f) Cyclic tensile stress-strain curves of the ionogel with 80 wt% IL at different strains. (g–i) Comparison of the mechanical properties between this work and other gel-like materials based on Young's modulus-fracture stress, toughness-fracture stress, and stretchability-fracture stress dependences.

enthalpy of ionogels are decreased with the IL content increased, which means the degree of crystallinity is reduced (Fig. 3b and Fig. S15). According to a simple calculating model (see Supplementary information), the relative crystallinity of ionogels, accompanied by thermal characteristics, is displayed in Table S3. The crystallinity is reduced from 30.5% to 9.4% when the IL content is increased from 30 to 80 wt%. Therefore, the crystallite size and crystallinity are synchronously decreased in the ionogel, resulting in a decreased melting temperature (Fig. 3b). Meanwhile, the structural information can be simultaneously observed in the SAXS results. The peak corresponds to the phase separation of crystalline and amorphous regions. When the IL content is increased, the intensity of the peak is reduced, which also means the degree of crystallinity is reduced, and the compatibility between the copolymer and IL is promoted (Fig. 3c). In addition, the location of the peak shifts to the left with increasing IL content, indicating an increased mean distance of the adjacent crystallites. The increased miscibility can be further characterized by SEM. When the IL content is low (e.g., 30 and 40 wt%), the surface of the ionogel is rough and uneven, illustrating the phase separation of the polymer and IL (Fig. S16a–d). With increasing the IL content to a high value (e.g., 70 and 80 wt%), a smooth surface is observed (Fig. S16e, f). However, the cross-sectional SEM micrographs display high compatibility between the polymer and IL inside the ionogels (Fig. S17), which is also confirmed by the elemental analysis (Fig. S18). This phenomenon, accompanied by SAXS results, reveals high miscibility between the copolymer and IL. The structure of ionogels can be further confirmed by FTIR (Fig. 3d). The band at 840 cm^{-1} is assigned to the formation of the β-phase crystal, while most bands assigned to the α-phase crystal have vanished. Therefore, our theoretical prediction that the suitable ratio of VDF can generate the appropriate amounts of crystalline regions and amorphous areas, is confirmed by the above structural analysis. Then, the network of the ionogel can be crosslinked by strong crystallization interaction and weak ion-dipole interaction, and the ionogel with high mechanical strength and good stretchability is obtained.

In situ two-dimensional (2D) WAXS and SAXS experiments were further carried out to analyze the structural transition of

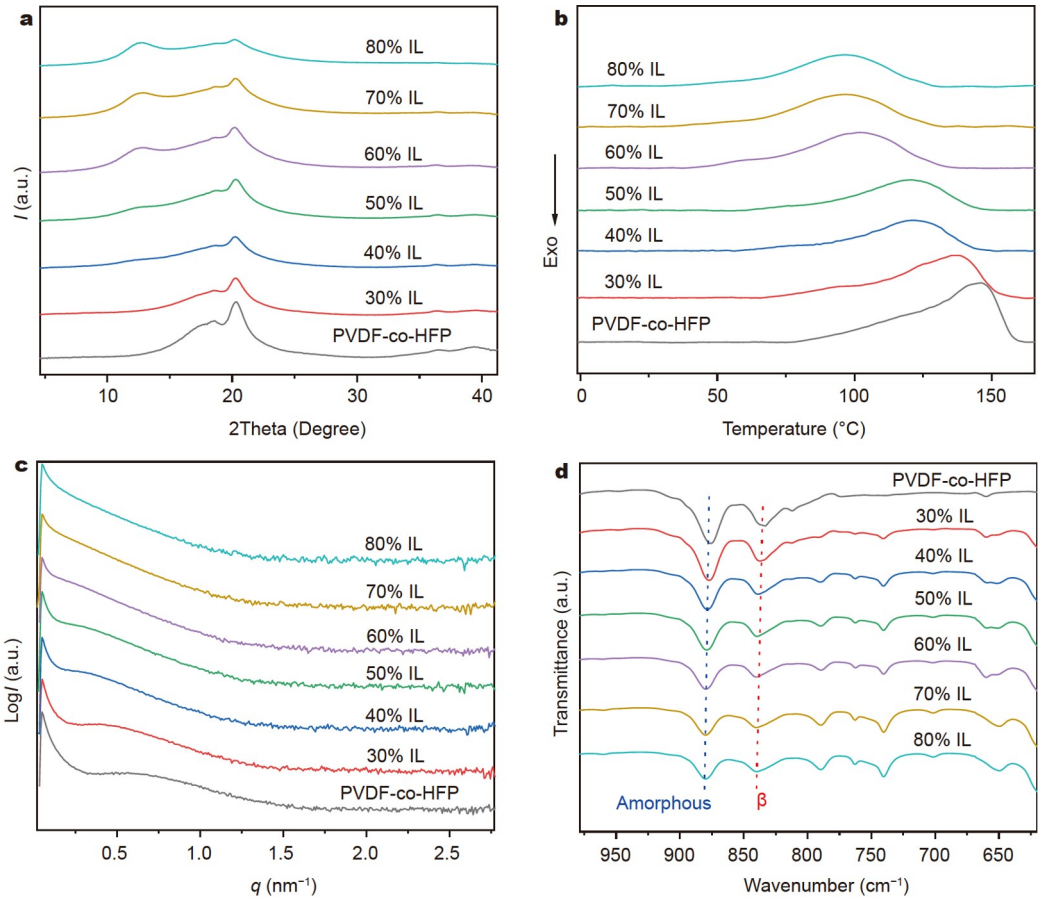

Figure 3 (a) WAXS, (b) DSC, (c) SAXS, and (d) FTIR results of ionogels with different IL contents.

ionogels in the loading and unloading process. There is no orientation of the crystals in the ionogel based on the uniform diffraction rings in the WAXS profile. When the sample is stretched less than 200%, the electron density distribution in the ionogel remains unchanged (Fig. S19a). However, when the sample is further stretched (above 300% strain), the two diffraction rings disappear, and a new diffraction ring at 5.1° appears. We think that the disappearance of the two diffraction rings means that the crystallite is broken, and the new peak corresponds to the diffraction of destructed crystallites. At the same time, the diffraction ring corresponding to the alternating amorphous and crystalline domains in the SAXS profile is also missing, which further confirms the above speculation about the destruction of crystallites. 1D integrated curves of the diffraction rings indicate the disappearance of the original diffractions and the formation of the new diffraction when the strain is changed from 0 to 400% (Fig. S19b, c). Hence, there is a stress-induced disaggregation behavior in the ionogel, which is different from the stress-induced crystallization behavior when VDF content is 96 mol% (Fig. S5b). The stress-induced disaggregation behavior has been found in the structural evolution of semi-crystalline polymers [56,57]. Lin's group [58] found that the disaggregation or amorphization of lamellar crystals can be induced in low-oriented or isotropic samples by pulling out chains from crystals. Men's group [59] also found a stress-induced disaggregation-recrystallization process of the crystalline block in ethylene-octene copolymers. When the stretched sample is recovered (below 200% strain), the new diffraction rings at 5.1° disappear, and the original diffraction rings in the WAXS and SAXS profiles reappear (Fig. S19a). In particular, the diffraction intensity remains almost unchanged compared with the pristine sample (Fig. S19b, c).

Then, a structural model can be proposed to explain the structural transition in the loading and unloading process and the enhancing mechanism of mechanical properties. As shown in Fig. 1a, the crystalline and amorphous regions are alternatively arranged in the ionogel. Because of the existence of HFP, the crystallinity is low and the crystallite size is small, while the amorphous region accounts for a large part. The crystalline part will provide the ionogel with robustness, and the amorphous region will afford elasticity. When the ionogel is prepared, increasing the IL content will further decrease the crystallinity and crystallite size by plasticizing the crystallite into an amorphous polymer. In addition, IL ions will also intercalate into PVDF crystallites to enlarge the *d*-spacing value when the IL content is larger than 60 wt%. This behavior can increase the mobility of PVDF crystallites. When the ionogel is stretched, the energy can be firstly dissipated by the deformation of the elastic amorphous regions. Further stretching will induce the destruction of PVDF crystallites to dissipate more energy. After the crystallites are disaggregated in the stretching process, the ion-dipole interaction can further prompt the ionogel with increased elasticity to be stretched to a super-large strain [24,60]. In other words, the stress-induced disaggregation behavior bears responsibility for the excellent mechanical properties of the ionogel. When the stress is unloaded, the microstructure of the

ionogel experiences a reversible transition in the recovering process, namely stress-unloaded recrystallization, which can ensure the mechanical stability of the ionogel.

Self-healing, recycled, and self-recovery properties

The ionogel can be poured into different shapes with ease, indicating the potential in different application scenarios (Fig. 4a). Furthermore, the self-healing capability of the ionogel is also studied because polymer crystallization and ion-dipole interaction are both reversible with changing temperature. The cut film can quickly fuse after being treated at 120°C for 2 min. There is no crack in the thermal-treated three-color stripe, and the stripe is easy to be bent and stretched (Fig. 4b). The healed sample still maintains almost half of the mechanical performance of the original sample. The stress and elongation at break are 1.32 MPa and 790%, respectively, which are still superior to most ionogels (Fig. 4c and Fig. S20).

In addition, our ionogel can be easily recycled. The ionogel can be dissolved in DMF again and re-casted into a transparent gel. The recycled gel exhibits similar mechanical properties as the pristine gel. There is only a slight decrease in tensile strength and stretchability, which means the environmentally friendly ionogel can be reprocessed and reused (Fig. 4d).

Although our tough ionogel displays yielding and mechanical hysteresis in the successive loading-unloading cycle (Fig. S21), it can fully self-recover to the original state after being stored for 30 min (Fig. 4e). The residual strain-waiting time dependence shows that the recovery process includes a quick process and a slow process, which is similar to that of ionomers and polyampholyte hydrogels (Fig. S22) [40,61]. However, the recovery time of ionomers and polyampholyte hydrogels is much longer. The two-stage recovery process may result from the competition between strong PVDF crystallization and temporarily re-formed weak ion-dipole interaction in the unloading process. PVDF crystallization is dominant at high strains (strain >35%), which results in a quick recovery. At low strains (strain <35%), the effect of crystallization becomes non-dominant, and the temporarily re-formed ion-dipole interaction decelerates the recovery speed of polymer chains to the original state. However, the recovery speed can be greatly improved by breaking and organizing the re-formed ion-dipole interaction through thermal treatment (Fig. S22). Thus, the ionogels show high fatigue resistance even without chemical crosslinking.

Electrical properties and applications

The electrical properties of ILs are excellent, and ionogels have been applied in a wide range of fields as flexible materials. Therefore, the ionic conductivity of the ionogel, which is correlated with the IL content, was measured using EIS in this study. There is no semicircle in the Nyquist curves of the ionogels with high IL contents (Fig. S23). This phenomenon results from the slight capacitance effect because of the small dielectric relaxation of the ions, which can also be observed in other ionogels [15]. The intercept obtained by linear extrapolation of the straight line in the Nyquist curve can be regarded as the ionic resistance to calculate the ionic conductivity. Because the pure IL exhibits a high conductivity of 9.10 mS cm^{-1}, the samples have high ionic conductivities. The conductivity of the ionogel with 30 wt% IL is 1.46 × 10^{-3} mS cm^{-1}, while it will be increased to 5.17 mS cm^{-1} when the IL content is 80 wt% (Fig. 5a and Table S4). The comparison of ionic conductivities of different ionogels is displayed in Table S5.

With increasing temperature, the enhanced mobility of cations, anions, and polymer chains will further promote ionic conductivity. Therefore, the ionic conductivities of the ionogel with 70 and 80 wt% IL are also attractive in a wide temperature range (Fig. 5b). Vogel-Tammann-Fulcher (VTF)

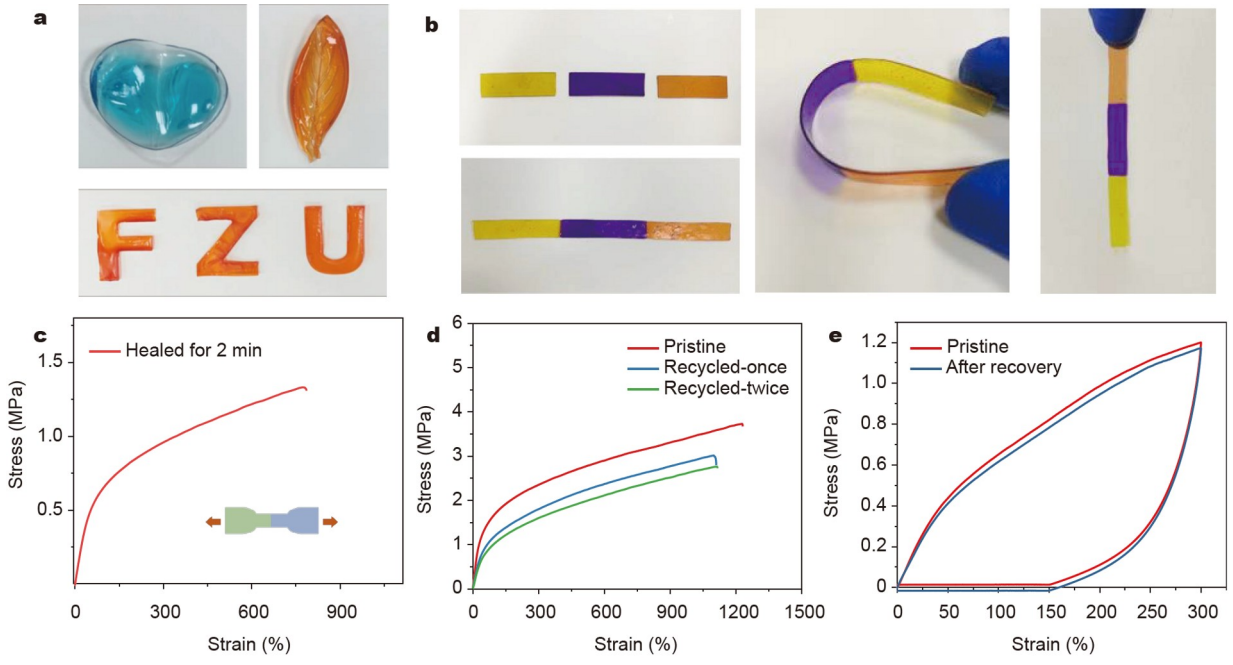

Figure 4 (a) Solution-cast ionogels with different shapes. (b) Self-healed three-color ionogel stripe. (c) Tensile stress-strain curve of the self-healed ionogel with 80 wt% IL. (d) Tensile stress-strain curves of the pristine ionogel and recycled samples. (e) Cyclic stress-strain curves of the pristine ionogel and recovered sample at a strain of 300%.

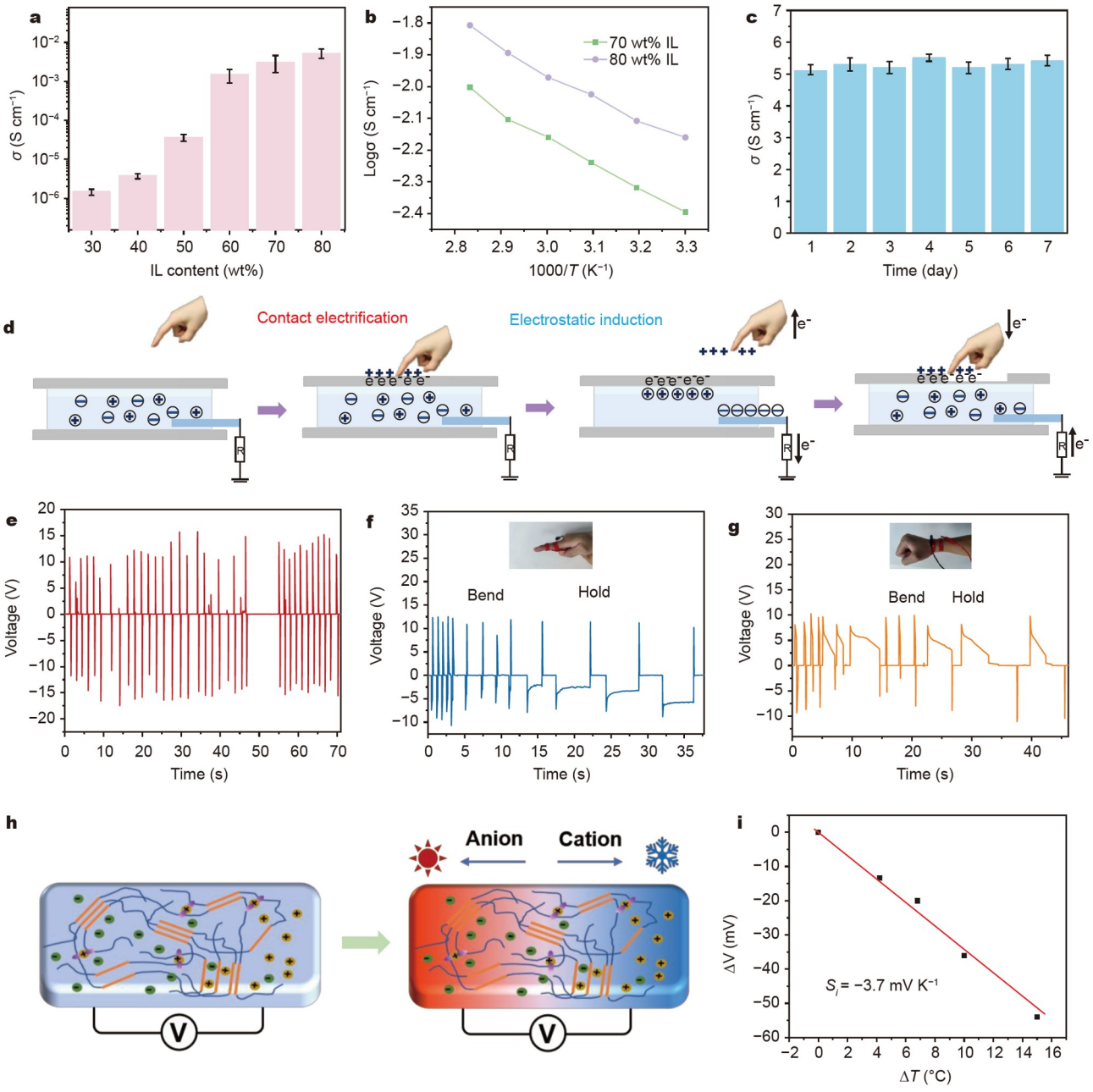

Figure 5 (a) Ionic conductivities of ionogels with different IL contents. (b) Ionic conductivities of ionogels with 70 and 80 wt% IL at different temperatures. (c) Ionic conductivity of ionogels with 80 wt% IL stored after seven days. (d) Schematic of the working principle of the iTENG. (e) Open-circuit voltage of the iTENG. Motion detections of the finger (f) and wrist (g) using the iTENG sensor. (h) Schematic of the ionic thermoelectric effect. (i) Thermopower of the ionogel with the IL content of 80 wt%.

equation below can be used to well fit the conductivity-temperature dependence,

$$\sigma = \sigma_0 \exp\left(\frac{-E_a}{R(T-T_0)}\right),$$

where σ_0, E_a, and T_0 represent the prefactor related to the charge carrier concentration, the activation energy related to the segmental motion, and the ideal glass transition temperature, respectively. The conductivity-temperature dependence of the ionogel exhibits a typical ion transportation behavior in polymer networks. The conductivity remains stable by placing the sample in the air for seven days (Fig. 5c). Moreover, the linear scanning voltammetry result reveals that the ionogel has a wide voltage window and good electrochemical stability (Fig. S24).

Then, an iTENG based on the ionogel was also fabricated to illustrate the potential application in energy harvesting and distinguishing the motion direction (Fig. 5d). A sandwich architecture with the ionogel sealed between two 3M VHB tapes was constructed to make the iTENG operate in the single electrode mode. When the iTENG is contacted by a gloved hand, the electrification will induce the same amount of positive and negative charges at the interface between the hand and VHB tape. When the hand is detached from the iTENG, the electrostatic induction will prompt the ion movement inside the

ionogel to balance the negative charges at the surface of the VHB tape. Then, the cations aggregate at the interface between the VHB tape and ionogel, and the anions gather at the interface between the ionogel and electrode. The electrons will further move from the electrode to the ground to form an electrical double layer until the negative charges in the VHB tape are screened. A reversed process will occur and the electrons will flow from the ground to the electrode if the gloved hand touches the iTENG again. When the iTENG is repeatedly pressed, alternating voltage and current are formed with a peak voltage of ~10 V and a peak current of ~0.05 μA (Fig. 5e and Fig. S25). The iTENG can also be used to detect motions because of its response to touches. When the iTENG is stuck on the finger, bending and straightening the finger will generate negative and positive voltages, respectively (Fig. 5f). Meanwhile, keeping the finger bent can generate a steady negative voltage. If the iTENG is used to detect the wrist movement, turning up or down the wrist can form a negative or positive voltage (Fig. 5g).

Keeping the wrist down can also result in a slow discharge process to zero-voltage, and the negative voltage can be re-formed when the wrist is raised again. Therefore, the motion direction can be monitored because of the directional electron flow.

Ionogels are also widely used as thermoelectric materials [15,62]. Since the anions and cations in the ionogel can directionally move under the temperature difference, a potential difference between the positive and negative electrodes can also be created, i.e., the Soret effect (Fig. 5h). As shown in Fig. 5i, with changing temperature, the thermopower of the ionogel with IL content of 80 wt% can reach −3.7 mV K^{-1}, with a good linear fitness of 0.99. Although there are only imidazolium cations and TFSI anions in the gel, the thermopower is relatively large. When the temperature difference is created, the anions move from the cold side to the hot side, while the cations move oppositely, which results in a negative thermopower. Then, the ionogel can be applied to temperature sensing, which is much more sensitive than the commercial thermocouple (0.04 mV K^{-1}) [63].

In addition, a flexible strain sensor was fabricated to test the potential application of the ionogel in wearable devices. The resistance of the ionogel is well responsive to the strain change (Fig. 6a, b). The relationship between the resistance change ($\Delta R/R_0$) and strain is linear with a high goodness-of-fit (0.998). The prepared sensor has high sensitivity, fast response, and good durability. The ionogel can be stuck on different joints to monitor body movements by recording the motion signals in real-time. Partial or full bending of the finger (Fig. 6c), and bending of the elbow (Fig. 6d) or knee (Fig. 6e) can be sensitively

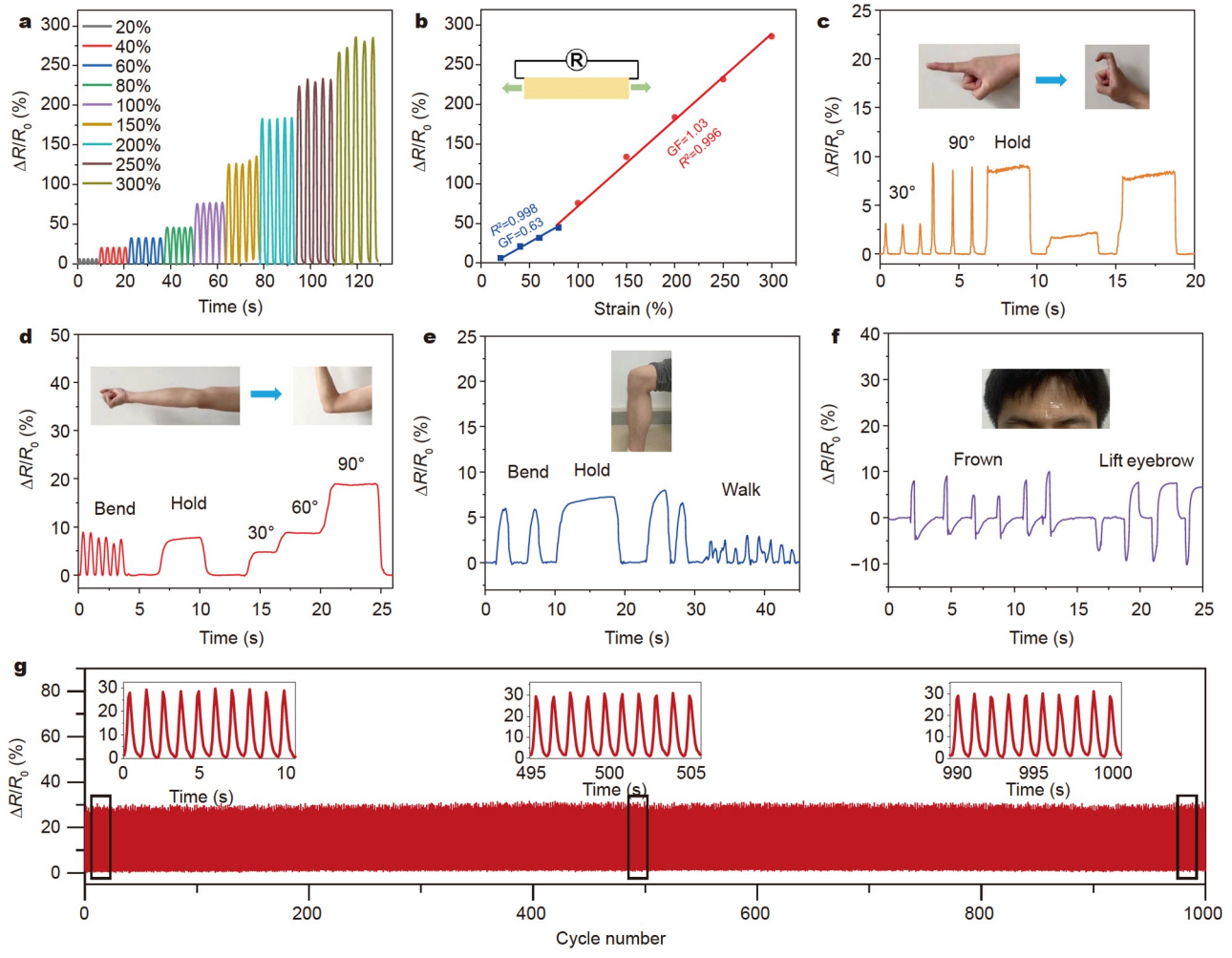

Figure 6 (a, b) Relative resistance changes of the ionogel with 80 wt% IL at different tensile strains. Real-time monitoring of human motions using the ionogel strain sensor: (c) finger, (d) elbow, (e) knee, and (f) forehead. (g) Stability test.

recorded by the ionogel-based strain sensor. Meanwhile, keeping the joints stationary, such as keeping the finger, elbow, or knee bent, can generate a real-time steady signal, which can be used to distinguish the motion state. The strain sensor can also be used to monitor subtle movements. When the ionogel is attached to the forehead, the frown can generate positive signals while lifting an eyebrow can produce negative signals (Fig. 6f). Then, a motion controller was used to measure the durability of the sensor. The resistance change displays excellent stability in the process of being stretched for 1000 cycles at the strain of 20% (Fig. 6g). Besides detecting conventional body movements, this sensor also has the potential to monitor the motion with high impact, in consideration of the high mechanical strength of the ionogel.

CONCLUSIONS

In conclusion, we have demonstrated a transparent ionic conductor with excellent strength/toughness/modulus, superior stretchability, high ionic conductivity, good fatigue resistance, quick self-recovery, recyclability, and self-healing ability that consists of a multiple crosslinking network and IL. A universal strategy is proposed to balance the polymer crystallization and ion-dipole interaction for addressing the trade-off between mechanical strength and stretchability. The stress-induced disaggregation of the polymer crystallization and formation of the ion-dipole interaction between amorphous polymer chains and IL are the main reasons for the extraordinary mechanical properties. We have put forward several application scenarios for wearable devices using this type of ionogel, including strain sensor, temperature sensing, and iTENG, with no need to worry about the evaporation during use like hydrogels. The strain sensor has high sensitivity, fast response, and good durability in detecting body motions, while iTENG can also be used to monitor the movement directions. In addition, the temperature sensor also has a hypersensitivity to temperature. Utilizing outstanding performance, optical transparency, and thermal stability, the ionogels offer broad prospects in the application of flexible iontronic devices. In addition, the construction strategy of ionogels in this study can also be employed to adjust other covalent or non-covalent interactions for preparing more high-performance ionogels.

Received 1 September 2022; accepted 14 October 2022; published online 1 January 2023

1 Tee BCK, Ouyang J. Soft electronically functional polymeric composite materials for a flexible and stretchable digital future. Adv Mater, 2018, 30: 1802560
2 Dinh Xuan H, Timothy B, Park HY, *et al.* Super stretchable and durable electroluminescent devices based on double-network ionogels. Adv Mater, 2021, 33: 2008849
3 Yiming B, Han Y, Han Z, *et al.* A mechanically robust and versatile liquid-free ionic conductive elastomer. Adv Mater, 2021, 33: 2006111
4 Tomé LC, Marrucho IM. Ionic liquid-based materials: A platform to design engineered CO_2 separation membranes. Chem Soc Rev, 2016, 45: 2785–2824
5 Chang Y, Wang L, Li R, *et al.* First decade of interfacial iontronic sensing: From droplet sensors to artificial skins. Adv Mater, 2021, 33: 2003464
6 Lin W, Kluzek M, Iuster N, *et al.* Cartilage-inspired, lipid-based boundary-lubricated hydrogels. Science, 2020, 370: 335–338
7 Gao G, Yang F, Zhou F, *et al.* Bioinspired self-healing human-machine interactive touch pad with pressure-sensitive adhesiveness on targeted substrates. Adv Mater, 2020, 32: 2004290
8 Zhuo S, Zhao Z, Xie Z, *et al.* Complex multiphase organohydrogels with programmable mechanics toward adaptive soft-matter machines. Sci Adv, 2020, 6: eaax1464
9 Gong JP, Katsuyama Y, Kurokawa T, *et al.* Double-network hydrogels with extremely high mechanical strength. Adv Mater, 2003, 15: 1155–1158
10 Zheng Y, Kiyama R, Matsuda T, *et al.* Nanophase separation in immiscible double network elastomers induces synergetic strengthening, toughening, and fatigue resistance. Chem Mater, 2021, 33: 3321–3334
11 Fukao K, Nakajima T, Nonoyama T, *et al.* Effect of relative strength of two networks on the internal fracture process of double network hydrogels as revealed by *in situ* small-angle X-ray scattering. Macromolecules, 2020, 53: 1154–1163
12 Tamate R, Watanabe M. Recent progress in self-healable ion gels. Sci Tech Adv Mater, 2020, 21: 388–401
13 Dong K, Liu X, Dong H, *et al.* Multiscale studies on ionic liquids. Chem Rev, 2017, 117: 6636–6695
14 Zhao D, Martinelli A, Willfahrt A, *et al.* Polymer gels with tunable ionic Seebeck coefficient for ultra-sensitive printed thermopiles. Nat Commun, 2019, 10: 1093
15 Cheng H, He X, Fan Z, *et al.* Flexible quasi-solid state ionogels with remarkable Seebeck coefficient and high thermoelectric properties. Adv Energy Mater, 2019, 9: 1901085
16 Yu D, Pan X, Bostwick JE, *et al.* Room temperature to 150°C lithium metal batteries enabled by a rigid molecular ionic composite electrolyte. Adv Energy Mater, 2021, 11: 2003559
17 Tang Z, Lyu X, Xiao A, *et al.* High-performance double-network ion gels with fast thermal healing capability *via* dynamic covalent bonds. Chem Mater, 2018, 30: 7752–7759
18 Lodge TP, Ueki T. Mechanically tunable, readily processable ion gels by self-assembly of block copolymers in ionic liquids. Acc Chem Res, 2016, 49: 2107–2114
19 Tang Z, Liu D, Lyu X, *et al.* Ultra-stretchable ion gels based on physically cross-linked polymer networks. J Mater Chem C, 2022, 10: 10926–10934
20 Kataoka T, Ishioka Y, Mizuhata M, *et al.* Highly conductive ionic-liquid gels prepared with orthogonal double networks of a low-molecular-weight gelator and cross-linked polymer. ACS Appl Mater Interfaces, 2015, 7: 23346–23352
21 Lan J, Li Y, Yan B, *et al.* Transparent stretchable dual-network ionogel with temperature tolerance for high-performance flexible strain sensors. ACS Appl Mater Interfaces, 2020, 12: 37597–37606
22 Tang B, White SP, Frisbie CD, *et al.* Synergistic increase in ionic conductivity and modulus of triblock copolymer ion gels. Macromolecules, 2015, 48: 4942–4950
23 Zhang S, Lee KH, Sun J, *et al.* Viscoelastic properties, ionic conductivity, and materials design considerations for poly(styrene-*b*-ethylene oxide-*b*-styrene)-based ion gel electrolytes. Macromolecules, 2011, 44: 8981–8989
24 Cao Y, Morrissey TG, Acome E, *et al.* A transparent, self-healing, highly stretchable ionic conductor. Adv Mater, 2017, 29: 1605099
25 Ren Y, Guo J, Liu Z, *et al.* Ionic liquid-based click-ionogels. Sci Adv, 2019, 5: eaax0648
26 Cao Z, Liu H, Jiang L. Transparent, mechanically robust, and ultrastable ionogels enabled by hydrogen bonding between elastomers and ionic liquids. Mater Horiz, 2020, 7: 912–918
27 Xu L, Huang Z, Deng Z, *et al.* A transparent, highly stretchable, solvent-resistant, recyclable multifunctional ionogel with underwater self-healing and adhesion for reliable strain sensors. Adv Mater, 2021, 33: 2105306
28 Weng D, Xu F, Li X, *et al.* Polymeric complex-based transparent and healable ionogels with high mechanical strength and ionic conductivity as reliable strain sensors. ACS Appl Mater Interfaces, 2020, 12: 57477–57485
29 Wang Y, Sun S, Wu P. Adaptive ionogel paint from room-temperature autonomous polymerization of α-thioctic acid for stretchable and healable electronics. Adv Funct Mater, 2021, 31: 2101494
30 Cho KG, An S, Cho DH, *et al.* Block copolymer-based supramolecular

ionogels for accurate on-skin motion monitoring. Adv Funct Mater, 2021, 31: 2102386
31 Wang M, Zhang P, Shamsi M, *et al.* Tough and stretchable ionogels by *in situ* phase separation. Nat Mater, 2022, 21: 359–365
32 Pan H, Zhang W, Xiao A, *et al.* Hierarchically ordered nanostructures of a supramolecular rod-coil block copolymer with a hydrogen-bonded discotic mesogen. Polym Chem, 2019, 10: 991–999
33 Lyu X, Huang H, Tang Z, *et al.* Efficient access to 3D mesoscopic prisms in polymeric soft materials. Macromol Rapid Commun, 2021, 42: 2100064
34 Lyu X, Tang Z, Li Y, *et al.* Tailored polymer particles with ordered network structures in emulsion droplets. Langmuir, 2021, 37: 509–515
35 Pan H, Zhang W, Xiao A, *et al.* Persistent formation of self-assembled cylindrical structure in a liquid crystalline block copolymer constructed by hydrogen bonding. Macromolecules, 2018, 51: 5676–5684
36 Zapata P, Mountz D, Meredith JC. High-throughput characterization of novel PVDF/acrylic polyelectrolyte semi-interpenetrated network proton exchange membranes. Macromolecules, 2010, 43: 7625–7636
37 Jansen JC, Friess K, Clarizia G, *et al.* High ionic liquid content polymeric gel membranes: Preparation and performance. Macromolecules, 2011, 44: 39–45
38 Zhang Y, Li M, Qin B, *et al.* Highly transparent, underwater self-healing, and ionic conductive elastomer based on multivalent ion-dipole interactions. Chem Mater, 2020, 32: 6310–6317
39 Li X, Cui K, Kurokawa T, *et al.* Effect of mesoscale phase contrast on fatigue-delaying behavior of self-healing hydrogels. Sci Adv, 2021, 7: eabe8210
40 Sun TL, Kurokawa T, Kuroda S, *et al.* Physical hydrogels composed of polyampholytes demonstrate high toughness and viscoelasticity. Nat Mater, 2013, 12: 932–937
41 Ameduri B. From vinylidene fluoride (VDF) to the applications of VDF-containing polymers and copolymers: Recent developments and future trends. Chem Rev, 2009, 109: 6632–6686
42 Mo J, Dai Y, Zhang C, *et al.* Design of ultra-stretchable, highly adhesive and self-healable hydrogels *via* tannic acid-enabled dynamic interactions. Mater Horiz, 2021, 8: 3409–3416
43 Lai YC, Wu HM, Lin HC, *et al.* Entirely, intrinsically, and autonomously self-healable, highly transparent, and superstretchable triboelectric nanogenerator for personal power sources and self-powered electronic skins. Adv Funct Mater, 2019, 29: 1904626
44 Yu Z, Wu P. Water-resistant ionogel electrode with tailorable mechanical properties for aquatic ambulatory physiological signal monitoring. Adv Funct Mater, 2021, 31: 2107226
45 Yiming B, Guo X, Ali N, *et al.* Ambiently and mechanically stable ionogels for soft ionotronics. Adv Funct Mater, 2021, 31: 2102773
46 Hou K, Zhao S, Wang D, *et al.* A puncture-resistant and self-healing conductive gel for multifunctional electronic skin. Adv Funct Mater, 2021, 31: 2107006
47 Nakajima T, Ozaki Y, Namba R, *et al.* Tough double-network gels and elastomers from the nonprestretched first network. ACS Macro Lett, 2019, 8: 1407–1412
48 Li S, Li Y, Wang Y, *et al.* Highly stretchable, elastic, healable, and ultradurable polyvinyl alcohol-based ionic conductors capable of safe disposal. CCS Chem, 2022, 4: 3170–3180
49 Hubbard AM, Cui W, Huang Y, *et al.* Hydrogel/elastomer laminates bonded *via* fabric interphases for stimuli-responsive actuators. Matter, 2019, 1: 674–689
50 Luo F, Sun TL, Nakajima T, *et al.* Oppositely charged polyelectrolytes form tough, self-healing, and rebuildable hydrogels. Adv Mater, 2015, 27: 2722–2727
51 Yu Z, Wu P. Underwater communication and optical camouflage ionogels. Adv Mater, 2021, 33: 2008479
52 Corkhill PH, Trevett AS, Tighe BJ. The potential of hydrogels as synthetic articular cartilage. Proc Inst Mech Eng H, 1990, 204: 147–155
53 Asaletha R, Kumaran MG, Thomas S. Thermoplastic elastomers from blends of polystyrene and natural rubber: Morphology and mechanical properties. Eur Polym J, 1999, 35: 253–271
54 Guan J, Shen J, Chen X, *et al.* Crystal forms and microphase structures of poly(vinylidene fluoride-*co*-hexafluoropropylene) physically and chemically incorporated with ionic liquids. Macromolecules, 2018, 52: 385–394
55 Jin ML, Park S, Kim JS, *et al.* An ultrastable ionic chemiresistor skin with an intrinsically stretchable polymer electrolyte. Adv Mater, 2018, 30: 1706851
56 Men Y, Rieger J, Strobl G. Role of the entangled amorphous network in tensile deformation of semicrystalline polymers. Phys Rev Lett, 2003, 91: 095502
57 Wang W, Jin Y, Ping P, *et al.* Structure evolution in segmented poly(ester urethane) in shape-memory process. Macromolecules, 2010, 43: 2942–2947
58 Habumugisha JC, Feng S, Iqbal O, *et al.* Stretch-induced structural evolution of pre-oriented isotactic polypropylene films: An *in-situ* synchrotron radiation SAXS/WAXS study. Polymer, 2021, 214: 123234
59 Sun Y, Fu L, Wu Z, *et al.* Structural evolution of ethylene-octene copolymers upon stretching and unloading. Macromolecules, 2013, 46: 971–976
60 Cao Y, Tan YJ, Li S, *et al.* Self-healing electronic skins for aquatic environments. Nat Electron, 2019, 2: 75–82
61 Varley RJ, Shen S, van der Zwaag S. The effect of cluster plasticisation on the self healing behaviour of ionomers. Polymer, 2010, 51: 679–686
62 Liu S, Yang Y, Huang H, *et al.* Giant and bidirectionally tunable thermopower in nonaqueous ionogels enabled by selective ion doping. Sci Adv, 2022, 8: eabj3019
63 Shiran Chaharsoughi M, Edberg J, Andersson Ersman P, *et al.* Ultrasensitive electrolyte-assisted temperature sensor. npj Flex Electron, 2020, 4: 23

Acknowledgements This work was supported by the National Key Research and Development Program of China (2020YFA0710303), the National Natural Science Foundation of China (22203015, U1905215, and 52072076), Fujian Science & Technology Innovation Laboratory for Optoelectronic Information (2021ZZ127), the Natural Science Foundation of Fujian Province (2021J01591), and Fuzhou University Testing Fund of precious apparatus (2022T006).

Author contributions Zhan W, Lyu X, and Luo ZZ designed and performed the experiments and analyzed the data. Lyu X and Zhan W conceived the work and co-wrote the manuscript. Zhang H assisted in the strain and self-healing measurements. All authors contributed to the general discussion.

Conflict of interest The authors declare that they have no conflict of interest.

Supplementary information Supporting data are available in the online version of the paper.

Weiqing Zhan received his Bachelor's degree from the School of Civil Engineering and Architecture, Nanchang Hangkong University in 2019. He is currently pursuing his Master's degree at the School of Materials Science and Engineering, Fuzhou University. His research interests focus on the preparation and application of high-performance polymer ionogels.

Xiaolin Lyu is an associate professor at the School of Materials Science and Engineering, Fuzhou University. He received his Bachelor's degree from Nanjing University in 2015 and PhD degree from Peking University in 2020. His current research involves ionic conducting polymer elastomers, and ionic thermoelectric conversion materials.

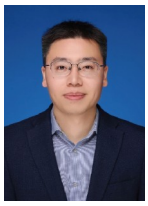

Zhong-Zhen Luo obtained his Bachelor's degree from Lanzhou University (2009) and PhD degree from Fujian Institute of Structure of Matter, Chinese Academy of Sciences (2014). He is currently a professor at the School of Materials Science and Engineering, Fuzhou University. His research focuses on thermoelectric materials, optoelectronic materials, and nonlinear optical crystals.

一种面向柔性离子电子学的超强韧、可拉伸的多功能离子凝胶

占卫青[1], 张浩琦[1], 吕晓林[1*], 罗中箴[1*], 于岩[1], 邹志刚[1,2]

摘要 离子凝胶由于良好的热稳定性、高离子传导性和非挥发性, 近年来引起了广泛的关注. 然而, 大部分离子凝胶并不能同时具备良好的机械强度和拉伸性, 因此其力学性能仍有待提高. 本工作将相互作用较强的聚合物结晶和较弱的离子偶极相互作用结合起来, 制备了一种超强韧且可拉伸的离子凝胶. 该离子凝胶具有高韧性、高断裂强度、高杨氏模量和良好的拉伸性. 此外, 该离子凝胶还具有良好的抗疲劳性、快速的自恢复性、高透明度、可回收性、自修复能力、高离子传导性和宽电化学窗口等特性. 同时, 其在摩擦纳米发电机、离子热电材料和应变传感器等离子电子器件中具有较大的应用潜力. 本工作通过可逆的强、弱相互作用, 为高性能离子凝胶的制备提供了一种新的方法.